

Chapter 3

Surface Functionalization by Laser-Induced Structuring



Juergen Reif

Abstract This chapter reviews the possibilities of functionalizing solid surfaces by laser irradiation—i.e. modifying the surfaces with respect to, e.g., wettability, optical properties, friction/wear-control, corrosion resistance, electrical properties. The functionalization occurs via the modification of surface morphology by the laser-induced formation of (regular) nano- to micro-textures. We present the different approaches to generate these patterns as well as their implication for specific functions obtained by this structuring and, finally, show some examples of applications.

3.1 Introduction

Materials surfaces play a paramount role in many aspects such as the optical appearance, mechanical properties like friction and wear, the interaction with the environment like wettability, corrosion, or adhesion. Also, chemical activity, e.g. in catalysis, is strongly dependent on the surface. The modification of solid surfaces to obtain new, functional properties is of considerable impact on the quality of modern engineering products and innovation [1, 2]. Such modification may be achieved, on the one hand, by coating the surface with a thin film providing the desired performance [3–5]. On the other hand, there is the possibility of modifying the actual surface morphology by the formation of new surface textures with feature size ranging from several hundred nanometers to the several ten microns, sometimes combining to form complex multi-scale hierarchical structures [6]. The patterns and their function often have their paradigm in nature and biology, with the most popular examples of the lotus leaf and its dirt-repelling hydrophobicity or of the colorful appearance of butterfly wings [7]. There are several techniques to achieve such surface patterning, including a combination of successive grinding, etching and chemical coating [8], or lithography [9], sometimes based on a template directly taken from a real

J. Reif (✉)

Brandenburgische Technische Universität – BTU Cottbus-Senftenberg,
Platz der Deutschen Einheit 1, 03046 Cottbus, Germany
e-mail: reif@b-tu.de

© Springer Nature Switzerland AG 2018

P. M. Ossi (ed.), *Advances in the Application of Lasers in Materials Science*, Springer Series in Materials Science 274,
https://doi.org/10.1007/978-3-319-96845-2_3

biological antetype [10]. A particular method is the replication from a mold formed by, e.g., diamond-machining [11]. Whereas most of these procedures employ multiple processing steps, surface nano-/micro-texturing can also be achieved by either self-organized pattern formation during thin film epitaxial growth [12] or by direct exposure to energetic irradiation, namely by ion, electron, or laser beams.

For charged particles beams, there are two typical ways of structuring: (a) direct-write lithography [13–16], and (b) relaxation from thermodynamic instability after ion-beam sputtering, where a large variety of regular to complex nano-patterns are attributed to a self-organized structure formation [17–19]. Surface morphology modification by intense laser pulses can be, similarly, differentiated into two main lines: (a) ablative lithography of multi-beam induced interference patterns [20], and (b) single beam formation of Laser-Induced Periodic Surface Structures (LIPSS) [21–28]. The latter two will be discussed in detail in the present chapter. We will start by showing some typical relations between surface textures—including laser-generated ones—and functionality. Then, we explicitly consider laser patterning and present several experimental approaches for their realization, together with current models explaining the interaction.

3.2 Functionality of Textured Surfaces

More or less regular surface patterns on the sub- to several micrometer scale result in numerous surface functionalities ranging from specific coloring over modified wettability [29], such as hydro- and oleo-phobicity or -philicity, special tribologic properties, wear-resistance, catalysis, modified adhesion. They can serve as templates for biological cell growth [30] and can stimulate surface enhanced Raman scattering [31, 32]. In the following, we present some typical surface functionalities and the patterns at their basis.

3.2.1 *Wettability*

One of the most important surface-morphology induced functionalities is, certainly, the modification of wettability, i.e. the controlled adjustment of liquid-repellent resp. liquid-attracting properties [1, 7]. The correlation is bio-inspired by the surface of the lotus leaf [7, 24, 33] (Fig. 3.1) or the rose petal [10].

Wettability, i.e. the capability of a solid to attract and spread or to repel a liquid on its surface, is of great importance both in daily life and, particularly, in technology. High wettability—for water called “hydrophilicity”—is required if a surface is to be covered by a thin liquid film, e.g. a lubricant or wet paint, to obtain an all-over coverage. Also the uniform spread of oil or water on a warm Teflon pan is due to this quality [34], despite its “cleaning effect” (the resulting wetting film provides a smooth, separating interface between the pan and the contents). The opposite

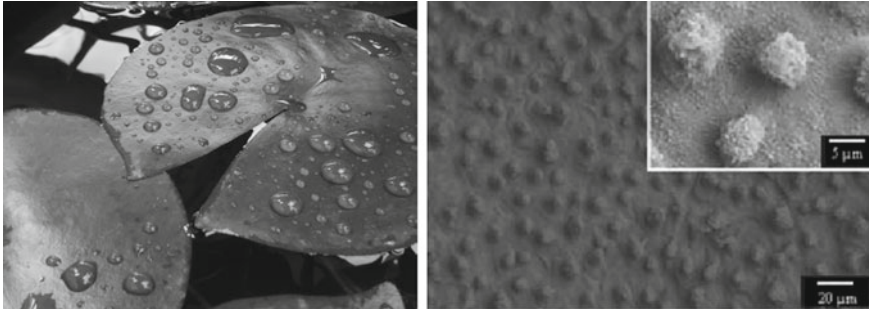


Fig. 3.1 Super-hydrophobic lotus leaf (from [33]). Left: photograph; right: SEM image of the lotus leaf surface

behavior of liquid repelling—for water called “hydrophobicity”—is important for effects like self-cleaning, e.g. of windshields, anti-icing of airplane wings, reduced corrosion, bacterial resistance.

The phenomenon of wettability is determined by the mutual interaction of the three phases: solid, liquid, and gaseous. It is, mainly, determined by attractive forces inside the liquid (cohesion) compared to interface forces between solid-liquid (adhesion) and liquid-gas. Typically, the latter are significantly weaker than the liquid internal binding, resulting in the confinement of a free liquid droplet because work against the internal binding is needed to increase the droplet surface. This effect is called surface tension; it controls the shape and size of a free liquid droplet, as described already in 1805 by Young [35]. At the droplet-surface interface, the competition of adhesive forces between the surface and the liquid, on the one hand, with cohesive forces within the liquid, on the other hand, is responsible for a minimization of the contact area. The shape of the droplet at the triple boundary (solid, liquid, gas) is then determined by a minimization of the total interface energy, γ [36], combining surface tension (liquid–gas, LG), droplet-surface adhesion (SL) and gas-surface adhesion (SG). It is characterized by the contact angle, θ , which is $>90^\circ$ for liquid repulsion (hydrophobicity) and $<90^\circ$ for attraction (hydrophilicity). At an *ideal* surface the contact angle is determined by Young’s Equation:

$$\cos \theta = \frac{\gamma_{SG} - \gamma_{SL}}{\gamma_{LG}} \quad (1)$$

This is, schematically, shown on the left panel in Fig. 3.2. For a *real* surface, however, we have to account for surface roughness, modifying the surface-liquid contact by, e.g., either increasing or reducing the efficient contact area, thus modifying the contact angle. These two possibilities are depicted on the center and right panels in Fig. 3.2.

It becomes immediately evident that the specific wettability is strongly influenced by the morphological structure of the surface roughness. Another important influence is due to the surface active area together with the surface charge distribution.

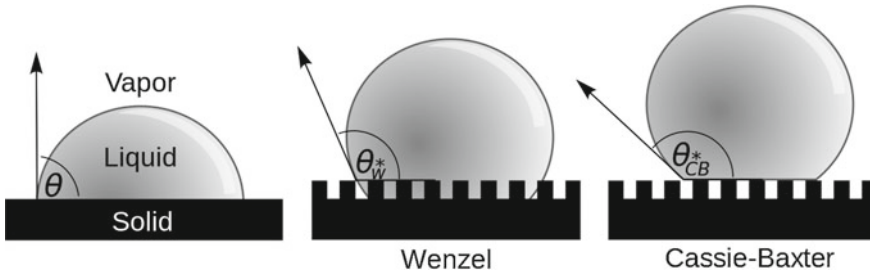


Fig. 3.2 Wetting states: Classical (Young) model for ideal surface (left); rough surface: Wenzel model, Cassie-Baxter model (super-hydrophobic). The wetting state is characterized by the contact angle θ

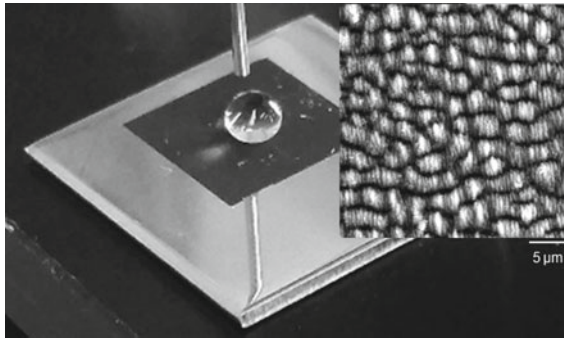


Fig. 3.3 Super-hydrophobic laser-processed steel surface

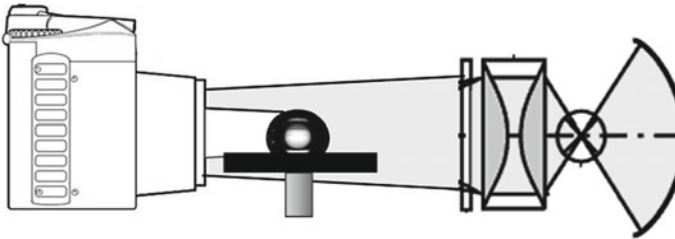


Fig. 3.4 Principle of sessile drop method for measuring contact angles: the liquid droplet sitting on the solid surface is homogeneously illuminated from the back; the resulting shadowgraph is recorded by a camera

Experimentally, super-hydrophobicity, similar to the lotus leaf, can be achieved by hierarchical (multi-scale) laser-modification of stainless steel [37] (cf. Fig. 3.3).

The contact angle can be, usually, measured optically by the sessile drop method [38] as shown in Fig. 3.4.

A particularly sensitive variation of the method consists in measuring the dynamic contact angle by changing the droplet volume. Then, a hysteresis of two different

contact angles is obtained: advancing by increasing the droplet volume and receding by reducing the droplet volume [39]. Generally, the receding contact angle is smaller and the advancing contact angle is larger than or equal to the static one.

3.2.2 Color

Similar to the feature of wettability, also the connection between surface micro-/nanostructure and color is bio-inspired. The most familiar examples are the multi-colored wings of butterflies [7, 40] (Fig. 3.5).

The phenomenon is based on the dispersion of white light transmitted (cf. Fig. 3.6) or reflected by optical gratings: due to interference, light incident on a grating of periodicity (line spacing) d is wavelength-dispersed and the fraction of wavelength λ continues to propagate under diffraction angle α for the first diffraction order (2):

$$\sin \alpha = \lambda/d \quad (2)$$

For given angles of illumination and observation, thus, different values of d result in different colors observed. The effective values of d do not only depend on the physical spacing but also on the orientation of the grating with respect to the plane of incidence (Fig. 3.7a) which is clearly obvious by the multi-color directional reflection from a compact disk with its circular grating pattern (Fig. 3.7b).

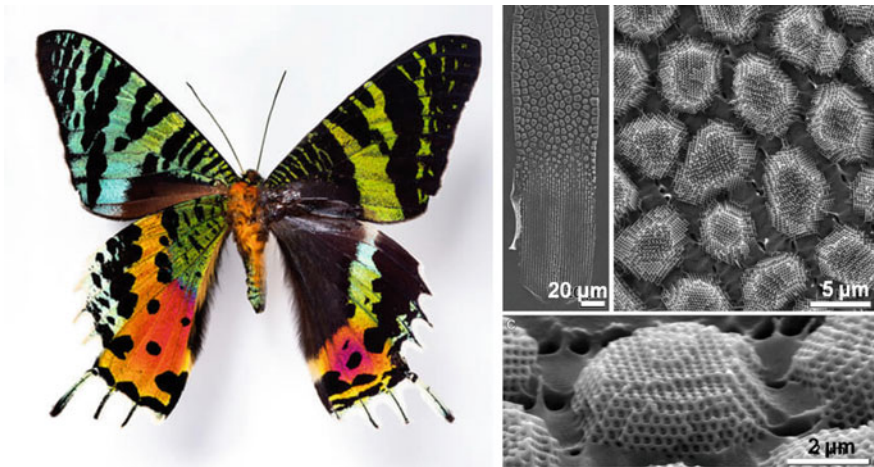


Fig. 3.5 Butterfly [Robert Clark, *National Geographic*] and SEM pictures of microstructures on a butterfly wing [40]

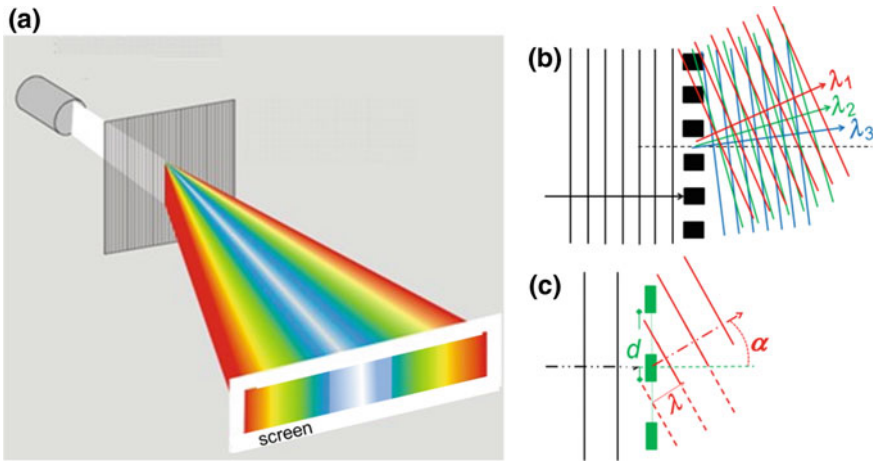


Fig. 3.6 Dispersion of white light by an optical grating. **a** Schematic (transmission); **b** Principle: incident white light (wave fronts and direction of propagation are indicated) is split and different wavelengths are diffracted into different directions; **c** Detail: for a line spacing d , light of wavelength λ is diffracted under angle α

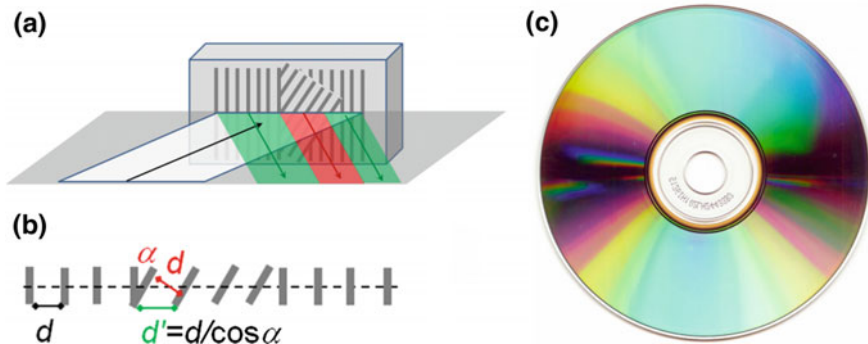


Fig. 3.7 Diffraction from identical but differently oriented—with respect to the plane of incidence—gratings. **a** Schematic; **b** Dependence of the effective grating spacing d' on grating orientation; **c** Diffraction from a compact disk (CD) with annular gratings

Indeed, such multi-color diffraction effect has been produced also by Laser-induced periodic structures (LIPSS) by Dusser et al. [41] (Fig. 3.8), where they could show, in addition, that the effect can be used for hidden marking.

A particular type of structure-induced “coloring” is the formation of deep black surfaces, such as carbon black [42, 43], or highly absorbing surfaces for applications in solar cells [44, 45]. The micro-/nano-structures responsible for that high absorption act two-fold: one the one hand, they simply increase the active surface considerably. But more important, on the other hand, is the multiple reflection and final trapping

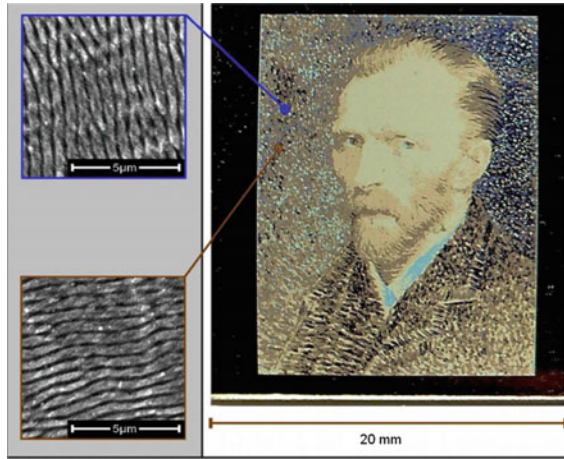


Fig. 3.8 Multi-color diffraction from a laser-structured surface with different LIPSS directions (from [41])

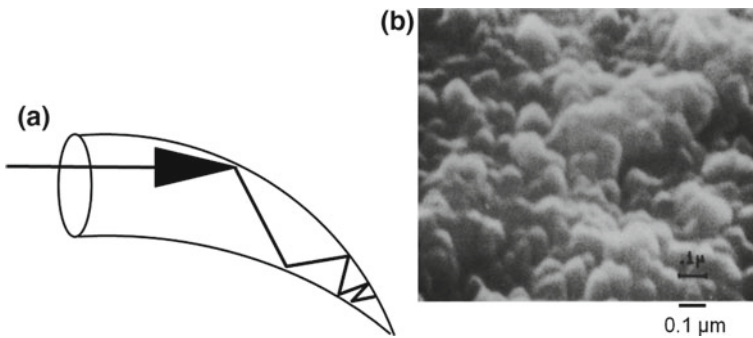


Fig. 3.9 Light-trapping by complex structures. **a** Wood's Horn; **b** "Black Chrome" (from [44])

inside the micro-/nano-structures like in a Wood's Horn (Fig. 3.9a). Typical structures consist of multiple pores [45] or multi-scale arrays of deep grooves or notches.

The creation of structural colors, notably black surfaces, by LIPSS has also been successfully reported [32]. As a particular application-related variant, "Black Silicon" has been produced, amongst others, by Eric Mazur's group [46].

3.2.3 Field Enhancement

Whereas, so far, surface functionality mostly because of depth modulation (depression) was considered, also sharp protrusions can have an important effect. In the presence of electric fields (static or electromagnetic) such tips or tip-arrays cause

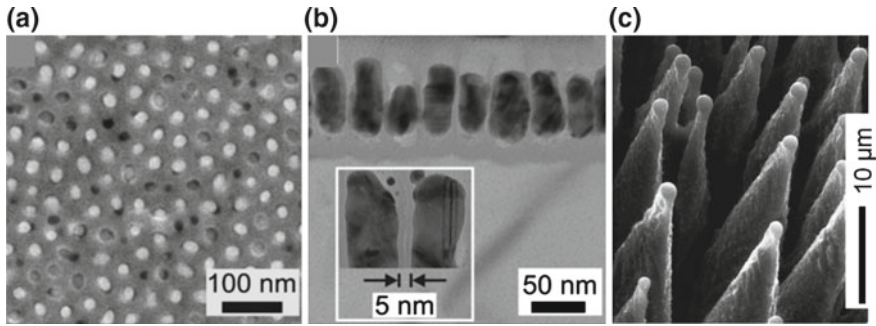


Fig. 3.10 Nanopillar arrays. **a** Ag-pillars on top of porous anodic alumina; **b** detail of the pillars in **(a)** (from [51]); **c** spikes on Si (100), produced by femtosecond LIPSS (from [53])

a considerable local field enhancement [47, 48]. This can be exploited as a very efficient, brilliant source of fast electron bunches [48, 49], e.g. for applications in ultrafast electron diffraction, crystallography, and microscopy [50]. The strong field enhancement in a tip-array can also increase the efficiency of surface enhanced Raman scattering (SERS) considerably [31, 51, 52]. Again, such tip-arrays can be easily fabricated also by LIPSS [53] (Fig. 3.10).

3.2.4 *Templates for Biological and Technological Films*

The main biological functionality of nanostructured surfaces is related to the formation of biologically active films [30, 54, 55] (Fig. 3.11)—or, contrarily, the suppression of their growth to avoid fouling [56]; the nanostructures can even serve to make titanium implants antibiotic [57].

An example for the formation of active films is the exploitation of ZnO nanostructures on silicon substrate as templates for the development of topography-mediated neuronal cultures [58]. It was demonstrated that the ZnO-templates can support neuronal cell growth and proliferation. Another effect is the stabilization and immobilization of enzymes on nano-structured surfaces [59, 60]. Natural nanostructures, such as diatoms with their outer shell of micro- and nano-porous silica, have been proposed as templates for bio/chemical sensors and biomimetic membranes [61]. Again, surface structures as templates for biofilms have also been produced by laser induced periodic surface structuring [62].

Not only for bio-films, also in Materials Science, can surface textures be used as templates to increase the functionality of films grown on these surfaces. As an example, epitaxially grown self-organized semiconductor nanostructures can serve as templates for very regular nanomagnet arrays [12].

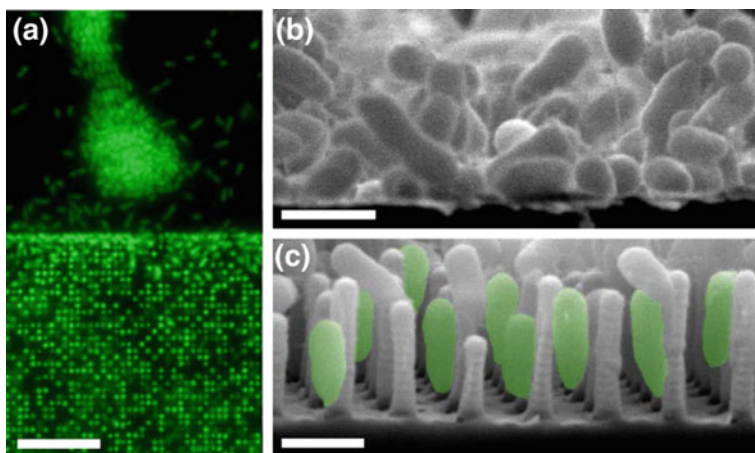


Fig. 3.11 Comparison of *P. aeruginosa* adhesion on structured and unstructured regions. **a** Fluorescence microscopy shows the different localized adhesion on flat region (upper) and structured region (lower), with an abrupt transition. **b** and **c** are corresponding cross-sectional SEM images, showing the strong difference in attachment morphology. The aligned cells in **(c)** are false-colored to highlight their orientation. Scale bars are 10 μm in **(a)** and 1 μm in **(b)** and **(c)**. (From [30])

3.3 Laser Patterning

In the following, we present the main methods to use laser techniques for regular surface texturing. In one way or the other, they are all closely related to the field of laser ablation: the light of, usually, strong laser pulses is absorbed by the target material and the resulting material response ranges from (surface) melting to massive material removal. In general, one can conceive two scenarios of responsible processes for pattern formation:

- (1) Local ablation after a patterned irradiation, very similar to lithography, using electron or ion beams [13–16], or local direct writing; one typical example is mask projection of excimer laser irradiation [63] (a; cf. Fig. 3.12), another approach is generating the pattern by multi-beam interference (b; Sect. 3.1).
- (2) Surface structuring by irradiation with a single beam (laser-induced periodic surface structures; LIPSS) [21–27].

3.3.1 Multi-beam Interference and Ablation

The most obvious way to generate mask-less patterned irradiation, as required for scenario (1b), is the illumination by interference of two or more beams, hitting the sample from different directions [20, 64–66] (Fig. 3.13).

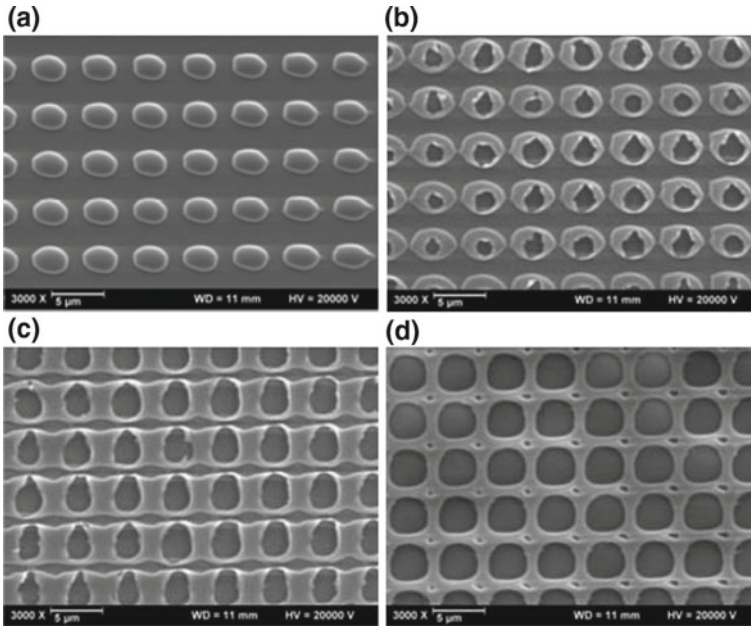
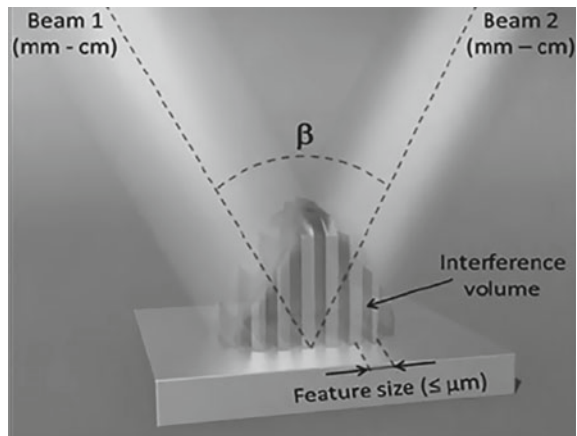


Fig. 3.12 Patterned 90 nm thick SiOx film; laser parameters: 248 nm, 1 pulse; structure period: 4.7 μm (from [63]). Fluence: **a** 180 mJ/cm², **b** 190 mJ/cm², **c** 200 mJ/cm², **d** 220 mJ/cm²

Fig. 3.13 Incident fluence modulation by interference pattern (from [64])



A typical example of such multi-beam-interference patterning is shown in Fig. 3.14 [66, 67]: an array of several parallel coherent beams is derived from a single laser in a diffractive optical element (DOE) and, then, focused to interfering overlap at the sample.

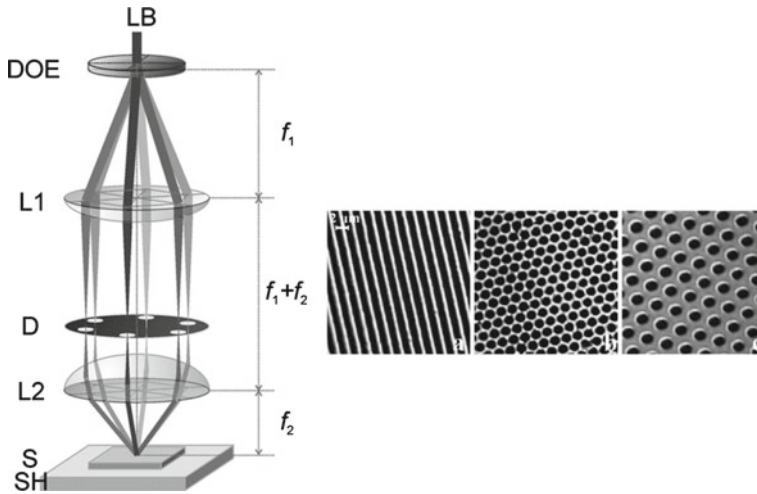


Fig. 3.14 Multi-beam-interference patterning. The left panel presents the principal set-up with the incident laser beam split into, here, six parallel beams by a combination of DOE and imaging lens. After spatial filtering, the beams are refocused to overlap on the sample. The right panels show micrographs of three typical patterns, obtained by interference of two, three, and six beams, respectively (from [67])

3.3.2 *Single-Beam Laser Induced Periodic Surface Structures (LIPSS)*

The phenomenon of surface morphology modification by incidence of a single laser beam was first observed already in 1965, shortly after the realization of the first laser, by Birnbaum [68]. In the beginning, this “surface damage” was mostly considered as an unwanted, though inevitable, trouble in materials processing as well as for optical components used with high power lasers [69, 70]. It was not before two decades later, that the phenomenon was studied in its own right [21, 71–77]. The next progress was the formation of sub-wavelength structures induced by ultrafast lasers [27, 78], again almost two decades later, initiating still ongoing research. This time, the emphasis is no longer on the damage aspect but, instead, growing interest is focused on possible, positive applications of the generated surface patterns, as indicated above in Sect. 3.2.

Nevertheless, the first experiments of femtosecond-LIPSS were concentrated on the effect as such. The first experiments investigated the surface morphology produced on a single interaction spot with diameters ranging from a few to more than 100 μm (cf. Fig. 3.15).

The effect is observed on a wide range of solid state materials [22], such as dielectric insulators [27], semiconductors [79], metals [80], and polymers [77, 81]. The irradiation is always close to the macroscopic ablation threshold, and the surface-morphology modification appeared as well after very few pulses [82, 83] (or even a single pulse [84–86]) as only after many thousand pulses [27].

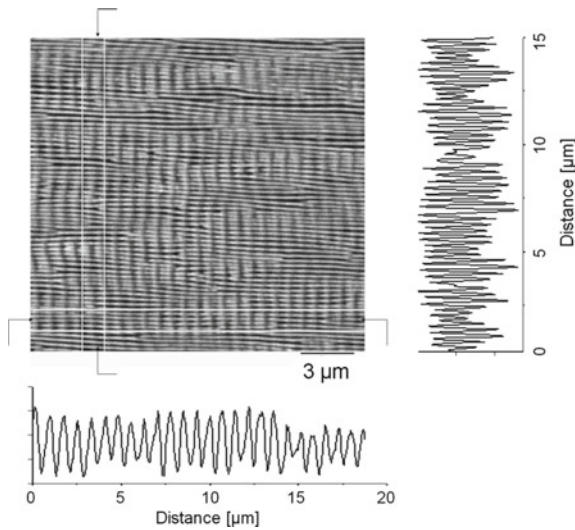


Fig. 3.15 Typical LIPSS pattern at the bottom of a 100- μm spot on a BaF_2 crystal surface, irradiated by 43,000 pulses from an amplified Ti:Sapphire Laser (800 nm wavelength; 100 fs pulse duration; $1 \text{ J}/\text{cm}^2$ fluence {90% of ablation threshold}; polarization vertical). Note that two periodic structures of different periodicity Λ (one of the order of the laser wavelength λ , the other one of about $\lambda/10$) are superimposed perpendicularly. The horizontal and vertical AFM traces, recorded in the indicated stripes, show the periodicities $\Lambda_1 \approx 690 \text{ nm}$, $\Lambda_2 \approx 280 \text{ nm}$. (From [27])

All experiments show that the LIPSS orientation is strongly determined by the polarization of the laser beam (Fig. 3.16a–e), with a few exceptions where surface scratches or similar irregularities can override the polarization dependence (Fig. 3.16f, g).

The laser-generated morphology can exhibit a variety of different appearances:

- (1) Very narrow, regular lines (for linear polarization) or spherical dots for circular polarization; cf. Fig. 3.16) with a feature size in the 100-nm range, well below the diffraction limit;
- (2) Wider periodic, parallel lines with a spacing close to the laser wavelength;
- (3) An array of larger irregular slabs of several- μm size, separated by deep trenches (similar to a dried-out river bed);
- (4) A regular array of conical tips, with spacing and size in the μm -range.

For convenience, the different features have been termed [22, 79] “HSFL” (high spatial frequency LIPSS) resp. “LSFL” (low spatial frequency LIPSS) for types 1 resp. 2 (cf. Fig. 3.15); “groves” (type 3), and “spikes” (type 4) (cf. Fig. 3.17). In general, HSFL and LSFL are oriented perpendicular to each other, a typical example is shown in Fig. 3.15.

An crucial parameter, affecting feature type and size appears to be the total dose of absorbed energy, i.e. the laser fluence and the number of superimposed laser shots

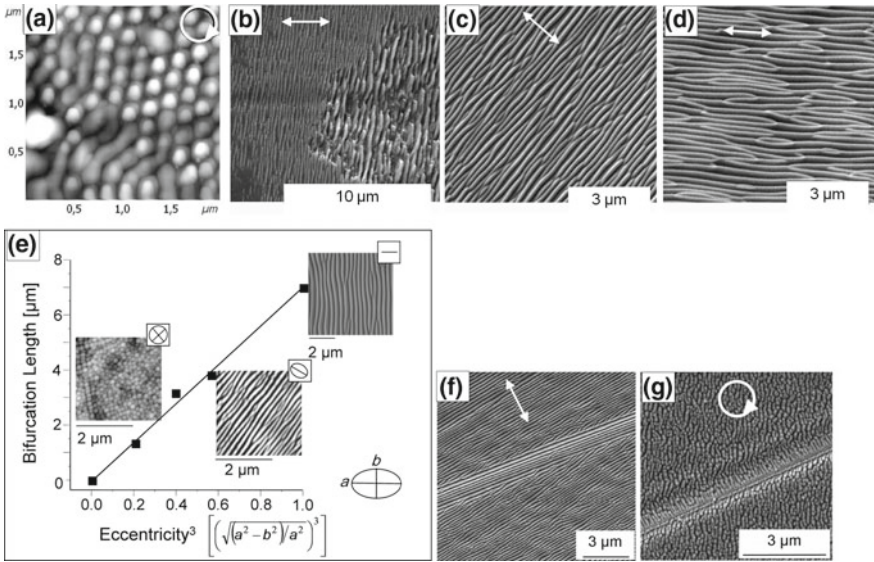


Fig. 3.16 Polarization dependence of LIPSS orientation. The respective polarization, circular in **a** [87] and linear in **b–d** [26] is indicated by the white arrows. **e** shows the effect of elliptical polarization [88]. In **f, g**, the influence of macroscopic scratches on the surface is shown, overriding the polarization dependence [89]

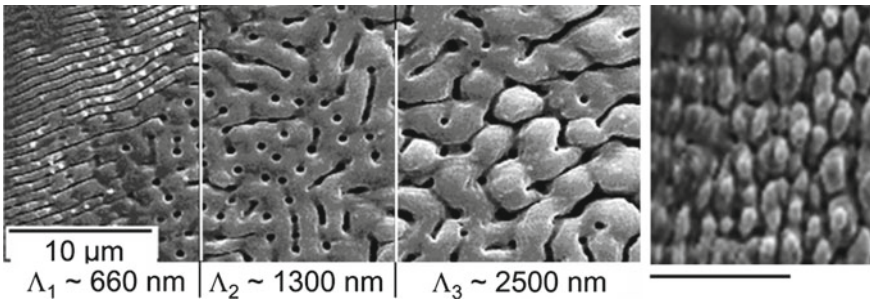


Fig. 3.17 LIPSS on silicon. The three areas on the left [90], showing LSFL and grooves, are from one single spot with Gaussian profile from the edge (left) to the center; the right panel shows spikes [91]. The scale is the same on all panels

[91–93]. This can be seen in Fig. 3.17 where the increasing intensity within the Gaussian spot profile results in a transition from LSFL to grooves

An important step towards an application of LIPSS structures was achieved by the discovery that it is possible to coherently modify larger areas by scanning the laser across the sample surface [94–97] (Fig. 3.18).

In general, there are two scanning methods as shown in Fig. 3.19: (a) Keeping the target fixed in position and scanning the laser spot by means of a pair of orthogonally

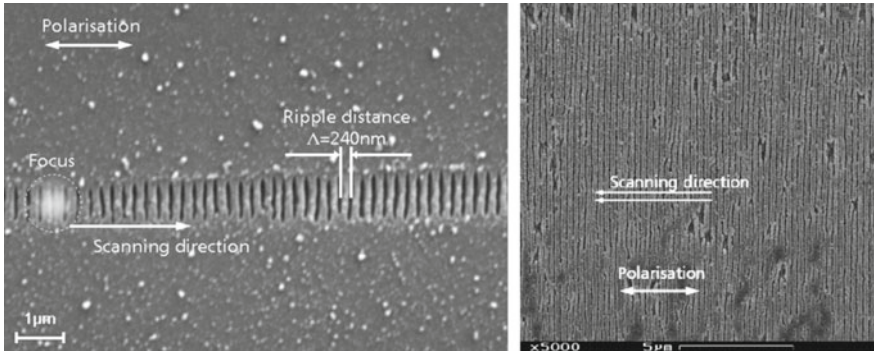


Fig. 3.18 Coherently continued ripples by scanning parallel to the polarization on fused silica. Left: single track: right: coherently continued ripples in 2D by scanning several tracks with an offset of 400 nm (one spot diameter) (from [96])

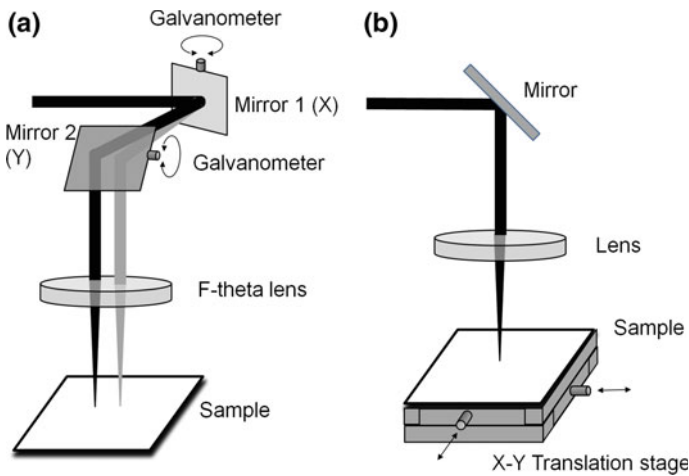


Fig. 3.19 Schematic of two methods for large area scanning. **a** Galvo scanning head and fixed sample, **b** fixed spot and mechanically scanning sample

moving mirrors (“scanning head”); the moving beam is, then, focused onto the target by an F-theta (telecentric) lens. (b) Keeping the laser spot fixed and moving the target, mounted on a set of precision translation stages.

Both techniques bear their individual advantages: procedure (a) allows a very high scanning speed, usually controlling the mirror motion by a galvanometric drive (galvoscaners); further, it allows a very compact and rigid set-up when using a commercial scanning head. Method (b) allows very large target areas to be covered, depending only on the translation stage size and precision; however, it is, generally, much slower and may be less compact; therefore, it is, mostly, used for laboratory application.

Typically, the full surface is covered by first writing lines along one direction (e.g. “X”) followed by adjacent tracks, displaced in the other direction (e.g. “Y”). Then, there are two further options: writing the lines either along or perpendicular to the laser polarization. Generally, it turns out that scanning normal to the ripples direction, i.e., usually, along the polarization, yields more regular patterns than the other sense. Another important parameter for the pattern quality is the scanning speed, or more precisely its ratio to the repetition rate, yielding longitudinal pulse overlap and, thus, the effective number of pulses acting on one spot area. A similar role is played by the scanning pitch, i.e. the separation of adjacent tracks (or lateral pulse overlap). The importance of these parameters becomes evident when considering the dose-dependence of the generated patterns (cf. Figs. 3.15 and 3.17).

3.3.2.1 LIPSS and Functionality

As was already addressed in Sect. 3.2, most of the functional nano-structuring can be, easily, achieved by LIPSS formation. Here, we just want to compile, again, the relevant features. It should be noted that, since LIPSS functionality only involves the surface of the modified material, usually very short laser pulses in the femto- or picosecond range are used to avoid thermal effects in the target volume [98]. A comprehensive review on LIPSS-functionalized surfaces can be found in [22–24, 32].

A Wettability

The modification of surface wettability by LIPSS was first reported in 2006 by the FORTH group on silicon [99] and by Groenendijk and Meijer [100], who patterned a stainless steel surface to become super-hydrophobic (cf. Fig. 3.20). Such surface could, subsequently, be used as a mould for plastic replicas exhibiting similar hydrophobicity.

There have been many approaches since then, showing, e.g., an improvement of hydrophobicity by chemical alkylsilane post-treatment [102] or the formation of hierarchical multiscale patterns [103]. Again, it appears that the irradiation dose plays an important role for controlling the functionality [37, 99]. In fact, is not only possible to make the surface (super-) hydrophobic but also hydrophilicity (super-wetting) can be achieved [23, 32, 37], even obtaining a surface where a water film creeps upwards against gravity [104, 105] (Fig. 3.21).

A peculiar effect, so far not fully understood, is the “aging” of processed metal surface [93]: even a multiscale-structured steel surface is not immediately super-hydrophobic but only develops this property after longer dwelling (from hours to days) in ambient atmosphere [37, 93, 103]. The most probable cause is some uncontrolled chemical modification, e.g. oxidation.

B Tribology

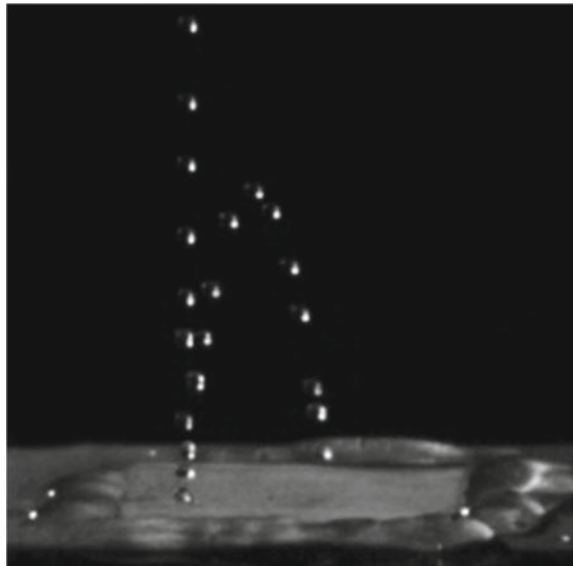
Closely related to the topic of modified wettability is the influence of LIPSS on the tribological properties of the treated surface. The underlying idea is two-fold: on the one hand, the depressions and grooves may serve to provide a reservoir for a possible lubricant; on the other hand, the reduced surface area, consistent of smooth, narrow ridges or tips, may reduce the resulting interaction between the surface and another body, rolling or sliding on that surface. A control of friction can have important implications: for a friction clutch in power transmission between a driving and a driven shaft it should be maximized; on the other hand, for wear reduction between moving surfaces, it should be reduced.

Consequently, the first proposal for an application of LIPSS intended to reduce friction and wear in a system of rapidly rotating hard disk and sliding head [106]. Following experiments on diamond like carbon (DLC) [107, 108], using femtosecond LIPSS, showed a reduction of both adhesive and lateral force (Fig. 3.22).

Chen et al. succeeded in reducing the friction coefficient of a SiC seal in water lubricant by about 20% [109] (Fig. 3.23).

Significant wear reduction on silicon [110] and on PEEK surface, a biocompatible thermoplastic for implanted joints, have been reported [111, 112]. Recently, Bonse et al. [113, 114] demonstrated that not only the LIPSS texture but also the contacting materials as well as possible lubricants play an important role.

Fig. 3.20 Super-hydrophobicity: falling droplet bounces back from a LIPSS surface [101]



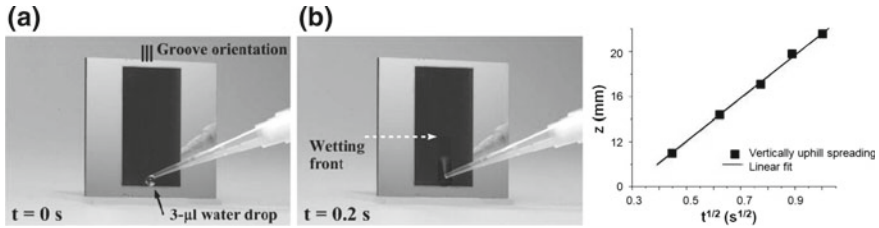


Fig. 3.21 Hydrophilicity: water droplet spreading up-hill (from [105])

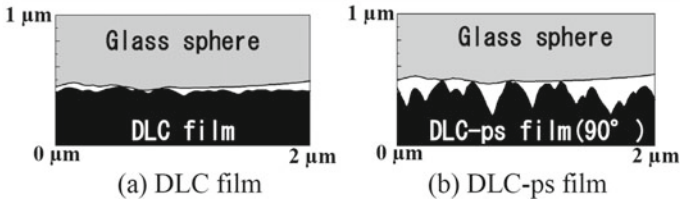


Fig. 3.22 Tribology: influence of LIPSS roughness on contact area (from [107])

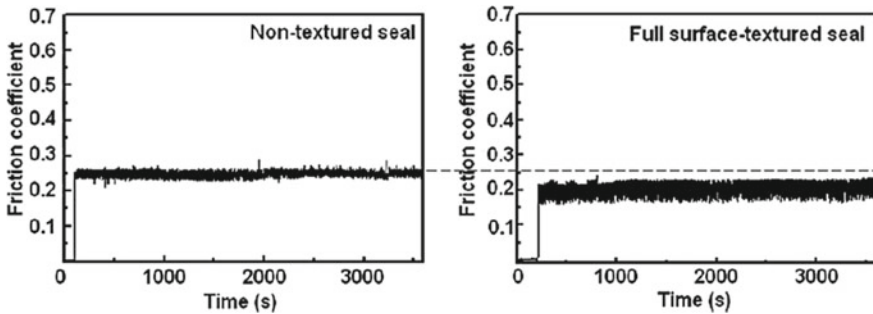


Fig. 3.23 LIPSS-reduction of friction coefficient of SiC in water lubricant (right). For comparison, the coefficient of the non-textured surface (left) is indicated by the dotted line (from [109])

C Color

Already in Sect. 3.2.2, examples are given for selective surface coloring by LIPSS formation (cf. Fig. 3.8; [41]). An impressive overview is presented in [32]. Particular interest appertains to the formation of black silicon, notably in order to optimize spectral absorption for photovoltaic applications. However, this has to be considered with care, since the structural surface modification is associated with the formation of electronic defects, significantly reducing the carrier lifetime [115]. Eric Mazur’s group succeeded in overcoming this problem by conducting the laser processing under SF₆ atmosphere [53] and subsequent annealing at 1200 K to remove hierarchical secondary structures [46] (Fig. 3.24).

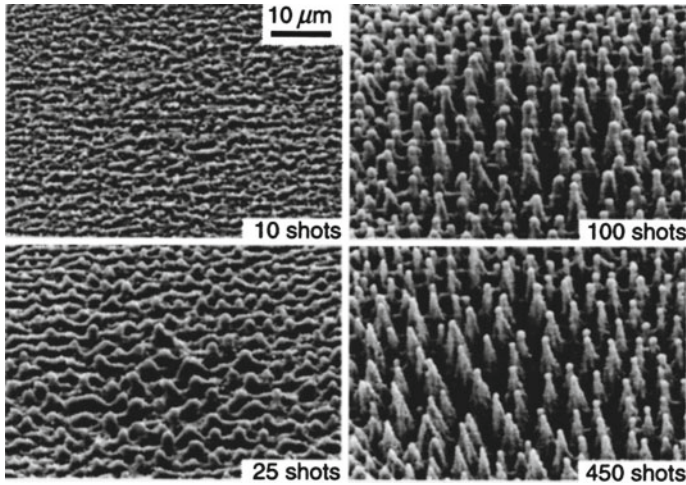
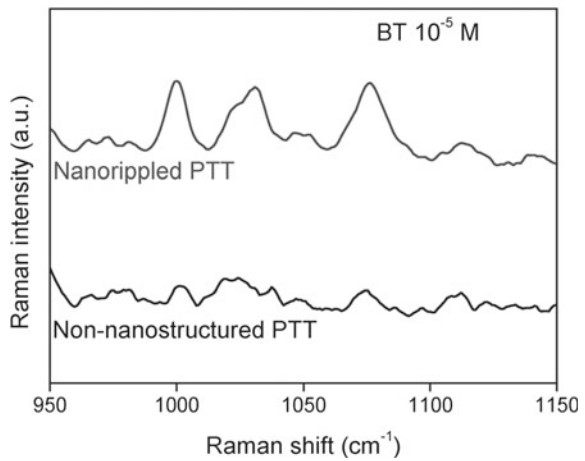


Fig. 3.24 “Black silicon”, formed by laser processing (from [46])

Fig. 3.25 Field enhancement of SERS on a LIPSS-textured surface (from [116])



D Field Enhancement/Surface Enhanced RAMAN Scattering

As indicated before, at sufficiently high irradiation dose the regular line-shaped LIPSS convert into an array of regular, sharp tips, capable to a considerable local electrical field enhancement. This can be exploited by using the array as a template for surface enhanced RAMAN scattering (SERS) [116–118] (Fig. 3.25).

E Templates for Biological and Technological Films

As generally holds for nanostructured surfaces (cf. Sect. 3.2.4), an interesting application of LIPSS patterned surface is the possibility of growing on top biological [119] or technological films [120] with peculiar features.

In the fields of medical and biological functionality, the main application concerns cell adhesion [121, 122]. There can be either a positive or, as well, a negative effect [62], depending on substrate and on biomaterial. A typical application concerns the optimization of titanium implants [82].

Another aspect applies to the LIPSS-template induced self-organized growth of ordered structures, both for biomaterials, e.g. directional cell spreading on titanium [123], and for technological materials, e.g. vertically aligned carbon nanofiber growth [120].

3.3.2.2 Lithographic Model: Laser-Plasmon Interference

The first approach to understand LIPSS formation was triggered by the apparent grating-like structures with a feature size close to the laser wavelength [21, 68–76]: the pattern was assumed to result from modulated ablation [68] following an illumination interference pattern between the incident wave and a surface-scattered wave [69, 72–74]. Keeping the basic idea of modulated ablation due to inhomogeneous energy deposition, the model was refined by ascribing the illumination pattern to interference between the incident wave and surface plasmon-polaritons, excited by the laser field. In order to apply this model also to non-conducting targets, a laser-induced transient high conduction-electron density was considered in a Drude-model for quasi-free electrons [124]. For more details see [22]. Though this model is very successful to predict all details of periodic surface structures of the LSFL type, its validity for other structures like HSFL, grooves, spikes is only very limited. The model is practically purely based on an assumption of particular electromagnetic field distributions occurring in the interaction, an active role of the material in structure formation is neglected, so far.

3.3.2.3 Surface Dynamic Model: Self-organization and Hydrodynamics

An alternative picture of the basic LIPSS formation mechanisms, developed by our group [26] has been triggered by the apparent similarity of LIPSS with patterns produced by self-organized epitaxy [12] or ion beam sputtering [19]. Our model is closely related to the concepts developed for the latter [17, 18] and assumes a much more active role of the material than the lithographic model (Sect. 3.3.2.2). The basic idea of the model postulates that the fast energy input to the target surface generates a state of transient thermodynamic instability (a state of disorder, similar but not equal to a melt) which, then, has to rapidly relax. This could be considered as a competition between surface roughening by erosion and surface smoothing

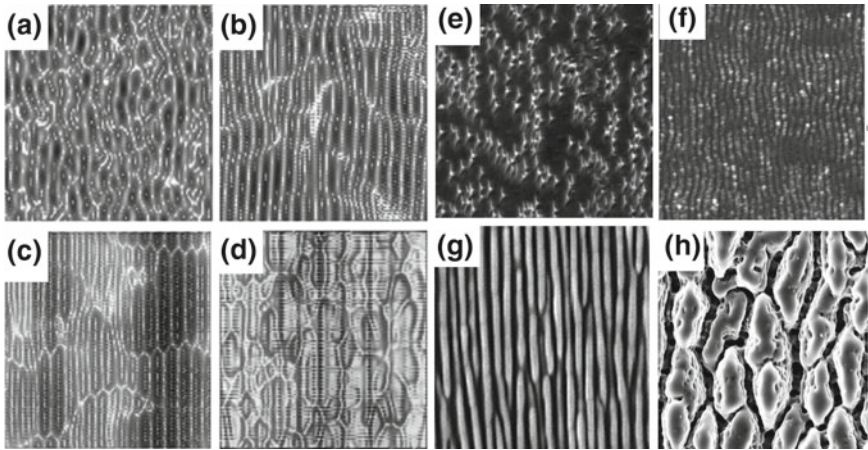


Fig. 3.26 Irradiation dose dependence of LIPSS: Comparison between simulated structures (surface dynamic model [126]; panels (a)–(d)) and experimental structures (panels (e)–(h)). The dose is gradually increased from (a) to (d) respectively from (e) to (h). Unfortunately, this is only a qualitative comparison, a quantitative comparison is not possible because of unknown material parameters, such as absorptivity, energy dissipation, etc

because of diffusion and surface tension, resulting in self-organization of the surface morphology. The process is described in the framework of nonlinear dynamics and can cover, by introducing several steps of nonlinearity as a function of feedback and degree of instability (as a function of absorbed energy dose), all types of structures observed (HSFL, LSFL, grooves, spikes), as is shown in Fig. 3.26. For more details, see [125].

References

1. K. Liu, L. Jiang, Metallic surfaces with special wettability. *Nanoscale* **3**, 825 (2011)
2. M. Woodson, J. Liu, Functional nanostructures from surface chemistry patterning. *Phys. Chem. Chem. Phys.* **9**, 207–225 (2007)
3. A. Zuzuarregui, M.C. Morant-Miñana (eds.), *Research Perspectives on Functional Micro- and Nanoscale Coatings* (IGI Global ACME, Information Science Reference; Hershey, PA, 2016)
4. J.T. Simpson, S.R. Hunter, T. Aytug, Superhydrophobic materials and coatings: a review. *Rep. Progr. Phys.* **78**, 086501 (2015)
5. M.F. Montemor, Functional and smart coatings for corrosion protection: a review of recent advances. *Surf. Coat. Technol.* **258**, 17–37 (2014)
6. J.V. Barth, G. Costantini, K. Kern, Engineering atomic and molecular nanostructures at surfaces. *Nature* **437**, 671–679 (2005)
7. H.-Y. Guo, Q. Li, H.-P. Zhao, K. Zhou, X.-Q. Feng, Functional map of biological and biomimetic materials with hierarchical surface structures. *RSC Adv.* **5**, 66901 (2015)
8. S. Ji, P.A. Ramahianti, T.-B. Nguyen, W.-D. Kim, H. Lim, Simple fabrication approach for superhydrophobic and superoleophobic Al surface. *Microel. Eng.* **111**, 404–408 (2013)

9. C. Acikgoz, M.A. Hempenius, J. Huskens, G.J. Vancso, Polymers in conventional and alternative lithography for the fabrication of nanostructures. *Eur. Polym. J.* **47**, 2033–2052 (2011)
10. S. Choo, H.-J. Choi, H. Lee, Replication of rose-petal surface structure using UV-nanoimprint lithography. *Mater. Lett.* **121**, 170–173 (2014)
11. E. Brinksmeier, R. Gläbe, L. Schönemann, *CIRP J. Manuf. Sci. Technol.* **5**, 1–7 (2012)
12. C. Teichert, Self-organized semiconductor surfaces as templates for nanostructured magnetic thin films. *Appl. Phys. A* **76**, 653–664 (2003)
13. A.A. Tseng, K. Chen, C.D. Chen, K.J. Ma, Electron beam lithography in nanoscale fabrication: recent development. *IEEE Trans. Electron. Packag. Manuf.* **26**, 141 (2003)
14. F. Watt, A.A. Bettiol, J.A. Van Kan, E.J. Teo, M.B.H. Breese, Ion beam lithography and nanofabrication: a review. *Int. J. Nanosci.* **4**, 269–286 (2005)
15. Y. Chen, Nanofabrication by electron beam lithography and its applications: a review. *Microelectron. Eng.* **135**, 57–72 (2015)
16. T. Som, D. Kanjilal (eds.), *Nano fabrication by Ion-Beam Sputtering: Fundamentals and Applications* (CRC Press, Boca Raton, Stanford, 2012)
17. J. Muñoz-García, L. Vázquez, R. Cuerno, J.A. Sánchez-García, M. Castro, R. Gago, *Self-Organized Surface Nanopatterning by Ion Beam Sputtering*, ed. by Z.M. Wang. *Toward Functional Nanomaterials* (Springer, Dordrecht, Heidelberg, London, New York, 2009), pp. 323–398
18. M. Castro, R. Cuerno, L. Vázquez, R. Gago, Self-Organized Ordering of Nanostructures Produced by Ion-Beam Sputtering, [arXiv:cond-mat/0506453v1](https://arxiv.org/abs/cond-mat/0506453v1) [cond-mat.stat-mech] 17 June 2005
19. F. Frost, B. Ziberi, A. Schindler, B. Rauschenbach, Surface engineering with ion beams: from self-organized nanostructures to ultra-smooth surfaces. *Appl. Phys. A* **91**, 551–559 (2008)
20. A.F. Lasagni, *Exploring the Possibilities of Laser Interference Patterning for the Rapid Fabrication of Periodic Arrays on Macroscopic Areas*, eds. by F.A. Lasagni, A.F. Lasagni. *Fabrication and Characterization in the Micro-Nano Range, Advanced Structured Materials 10* (Springer, 2011), pp. 1–27
21. H.M. van Driel, J.E. Sipe, J.F. Young, Laser-induced periodic surface structures on solids: a universal phenomenon. *Phys. Rev. Lett.* **49**, 1955–1958 (1982)
22. J. Bonse, S. Höhm, S.V. Kirner, A. Rosenfeld, J. Krüger, Laser-induced periodic surface structures—a scientific evergreen. *IEEE J. Sel. Top. Quantum Electron.* **23**, 9000615 (2017)
23. A. Vorobyev, C. Guo, Multifunctional surfaces produced by femtosecond laser pulses. *J. Appl. Phys.* **117**, 033103 (2015)
24. F.A. Müller, C. Kunz, S. Gräf, Bio-inspired functional surfaces based on laser-induced periodic surface structures. *Materials* **9**, 476 (2016)
25. K.C. Phillips, H.H. Gandhi, E. Mazur, S.K. Sundaram, Ultrafast laser processing of materials: a review. *Adv. Opt. Photonics* **7**, 684–712 (2015)
26. J. Reif, F. Costache, M. Bestehorn, *Self-organized surface nano-structuring by femtosecond laser processing; Chapter 9*, eds. by J. Perriere, E. Millon, E. Fogarassy. *Recent Advances in Laser Processing of Materials* (Elsevier, 2006) p. 275
27. J. Reif, F. Costache, M. Henyk, S.V. Pandelov, Ripples revisited: non-classical morphology at the bottom of femtosecond laser ablation craters in transparent dielectrics. *Appl. Surf. Sci.* **197–198**, 891–895 (2002)
28. K.M. Tanvir Ahmmed, C. Grambow, A.M. Kietzig, Fabrication of micro/nano structures on metals by femtosecond laser micromachining. *Micromachines* **5**, 1219–1253 (2014)
29. R. Blossey, Self-cleaning surfaces—virtual realities. *Nat. Mater.* **2**, 301–306 (2003)
30. A.I. Hochbaum, J. Aizenberg, Bacteria pattern spontaneously on periodic nanostructure arrays. *Nano Lett.* **10**, 3717–3721 (2010)
31. S. Kawata, V.M. Shalaev (eds.), *Tip Enhancement*, (*Adv. Nano-Optics Nano-Photonics 2*) (Elsevier, 2017)
32. A.Y. Vorobyev, C. Guo, Direct femtosecond laser surface nano/microstructuring and its applications. *Laser Photonics Rev.* **7**, 385–407 (2013)

33. J. Lin, Y. Cai, X. Wang, B. Ding, J. Yu, M. Wang, Fabrication of biomimetic superhydrophobic surfaces inspired by lotus leaf and silver ragwort leaf. *Nanoscale* **3**, 1258 (2011)
34. L. Gao, T.J. McCarthy, Teflon is hydrophilic. Comments on definitions of hydrophobic, shear versus tensile hydrophobicity, and wettability characterization. *Langmuir* **24**, 9183–9188 (2008)
35. T. Young, An essay on the cohesion of fluids. *Phil. Trans. R. Soc. London* **95**, 65–87 (1805)
36. K. Seoh, M. Kim, D.H. Kim, *Re-derivation of Young's Equation, Wenzel Equation, and Cassie-Baxter Equation Based on Energy Minimization*, ed. by M. Aliofkhazraei. *Surface Energy* (InTech open, 2015)
37. O. Varlamova, K. Hoefner, M. Ratzke, J. Reif, D. Sarker, Modification of surface properties of solids by femtosecond LIPSS writing: comparative studies on Silicon and Stainless Steel. *Appl. Phys. A* **123**, 725 (2017)
38. J.F. Padday, A.R. Pitt, Surface and interfacial tensions from the profile of a sessile drop. *Proc. R. Soc. London A* **329**, 421–431 (1972)
39. R. Tadmor, Line energy and the relation between advancing, receding, and young contact angles. *Langmuir* **20**, 7659–7664 (2004)
40. B.D. Wilts, B.A. Zubiri, M.A. Klatt, B. Butz, M.G. Fischer, S.T. Kelly, E. Spiecker, U. Steiner, G.E. Schröder-Turk, Butterfly gyroid nanostructures as a time-frozen glimpse of intracellular membrane development. *Sci. Adv.* **3**, e1603119 (2017)
41. B. Dusser, Z. Sagan, H. Soder, N. Faure, J.P. Colombier, M. Jurlin, E. Audouard, Controlled nanostructures formation by ultra fast laser pulses for color marking. *Opt. Express* **18**, 2913–2924 (2010)
42. J.-P. Donnet, T.-K. Wang, Surface microstructure of carbon black: advances in characterization by scanning tunneling microscopy. *Macromol. Symp.* **108**, 97–109 (1996)
43. W. Niedermeier, H. Raab, J. Stierstorfer, S. Kreitmeier, D. Göritz, The microstructure of carbon black investigated by atomic force microscopy. *Kautsch. Gummi Kunstst.* **47**, 799–805 (1994)
44. A. Ignatiev, P. O'Neill, G. Zajac, The surface microstructure optical properties relationship in solar absorbers: black chrome. *Solar Energy Mater.* **1**, 69–79 (1979)
45. Y. Yan, H.-C. Yuan, V.E. Yost, K. Jones, M. Al-Jassim, H.M. Branz, Microstructure and surface chemistry of nanoporous “Black Silicon” for photovoltaics, in *Proc. 35th IEEE Photovoltaic Specialists Conference Rec.*, pp. 2255–2257, 2010
46. C. Wu, C.H. Crouch, L. Zhao, J.E. Carey, R. Younkin, J.A. Levinson, E. Mazur, R.M. Farrell, P. Gothoskar, A. Karger, Near-unity below-band-gap absorption by microstructured silicon. *Appl. Phys. Lett.* **78**, 1850 (2001)
47. C.A. Spindt, A thin-film field-emission cathode. *J. Appl. Phys.* **39**, 3504 (1968)
48. S. Tsujino, F. le Pimpec, J. Raabe, M. Buess, M. Dehler, E. Kirk, J. Gobrecht, A. Wrulich, Static and optical field enhancement in metallic nanotips studied by two-photon photoemission microscopy and spectroscopy excited by picosecond laser pulses. *Appl. Phys. Lett.* **94**, 093508 (2009)
49. A. Mustonen, P. Beaud, E. Kirk, Th Feurer, S. Tsujino, Five picocoulomb electron bunch generation by ultrafast laser-induced field emission from metallic nano-tip arrays. *Appl. Phys. Lett.* **99**, 103504 (2011)
50. A.H. Zewail, 4D ultrafast electron diffraction, crystallography, and microscopy. *Annu. Rev. Phys. Chem.* **57**, 65–103 (2006)
51. H.-H. Wang, C.-Y. Liu, S.-B. Wu, N.-W. Liu, C.-Y. Peng, T.-H. Chan, C.-F. Hsu, J.-K. Wang, Y.-L. Wang, Highly Raman-enhancing substrates based on silver nanoparticle arrays with tunable sub-10 nm gaps. *Adv. Mater.* **18**, 491 (2006)
52. H. Ko, S. Singamaneni, V.V. Tsukruk, Nanostructured surfaces and assemblies as SERS media. *Small* **4**(10), 1576–1599 (2008)
53. T.-H. Her, R.J. Finlay, C. Wu, S. Deliwala, E. Mazur, Microstructuring of silicon with femtosecond laser pulses. *Appl. Phys. Lett.* **73**, 1673 (1998)
54. A. Karatas, A.H. Algan, Template synthesis of tubular nanostructures for loading biologically active molecules. *Curr. Top. Med. Chem.* **17**, 1555–1563 (2017)

55. A.K. Epstein, A.I. Hochbaum, P. Kim, J. Aizenberg, Control of bacterial biofilm growth on surfaces by nanostructural mechanics and geometry. *Nanotechnology* **22**, 494007 (2011)
56. M.V. Graham, N.C. Cady, Nano and microscale topographies for the prevention of bacterial surface fouling. *Coatings* **4**, 37–59 (2014)
57. F. Hizal, I. Zhuk, S. Sukhishvili, H.J. Busscher, H.C. van der Mei, C.-H. Choi, Impact of 3D hierarchical nanostructures on the antibacterial efficacy of a bacteria-triggered self-defensive antibiotic coating. *ACS Appl. Mater. Interfaces*. **7**, 20304–20312 (2015)
58. A. Kritharidou, Z. Georgoussi, C. Tsamis, E. Makarona, Zinc oxide nanostructures as low-cost templates for neuronal circuit. *Proc. SPIE* **8765**, 87650G (2013)
59. J. Kim, J.W. Grate, P. Wang, Nanostructures for enzyme stabilization. *Chem. Eng. Sci.* **61**, 1017–1026 (2006)
60. N. Carlsson, H. Gustafsson, C. Thörn, L. Olsson, K. Holmberg, B. Åkerman, Enzymes immobilized in mesoporous silica: a physical–chemical perspective. *Adv. Colloid Interface Sci.* **205**, 339–360 (2014)
61. W. Yang, P.J. Lopez, G. Rosengarten, Diatoms: self assembled silica nanostructures, and templates for bio/chemical sensors and biomimetic membranes. *Analyst* **136**, 42–53 (2011)
62. N. Epperlein, F. Menzel, K. Schwibbert, R. Koter, J. Bonse, J. Sameith, J. Krüger, J. Toepel, Influence of femtosecond laser produced nanostructures on biofilm growth on steel. *Appl. Surf. Sci.* **418**, 420–424 (2017)
63. D. Köhne, T. Fricke-Begemann, R. Weichenhain-Schriever, J. Ihlemann, Large area silica nano grids by homogeneous high resolution laser patterning of SiO_x-films. *JLMN* **10**, 158–161 (2015)
64. D. Huerta-Murillo, A.I. Aguilar-Morales, S. Alamri, J.T. Cardoso, R. Jagdheesh, A.F. Lasagni, J.L. Ocaña, Fabrication of multi-scale periodic surface structures on Ti-6Al-4 V by direct laser writing and direct laser interference patterning for modified wettability applications. *Opt. Lasers Eng.* **98**, 134–142 (2017)
65. M. Bieda, M. Siebold, A.F. Lasagni, Fabrication of sub-micron surface structures on copper, stainless steel and titanium using picosecond laser interference patterning. *Appl. Surf. Sci.* **387**, 175–182 (2016)
66. S. Indrišiūnas, B. Voisiat, A. Žukauskas, G. Račiukaitis, Direct laser beam interference patterning technique for fast high aspect ratio surface structuring. *Proc. SPIE* **9359**, 935003-1 (2015)
67. M. Gedvilas, B. Voisiat, S. Indrišiūnas, G. Račiukaitis, V. Veiko, R. Zakoldaev, D. Sinev, E. Shakhno, Thermo-chemical microstructuring of thin metal films using multi-beam interference by short (nano- & picosecond) laser pulses. *Thin Solid Films* **634**, 134–140 (2017)
68. M. Birnbaum, Semiconductor surface damage produced by ruby lasers. *J. Appl. Phys.* **36**, 3688–3689 (1965)
69. D.C. Emmony, R.P. Howson, L.J. Willis, Laser mirror damage in germanium at 10.6 μm. *Appl. Phys. Lett.* **23**, 598–600 (1973)
70. M. Siegrist, G. Kaech, F.K. Kneubühl, Formation of a periodic wave structure on the dry surface of a solid by TEA-CO₂ laser pulses. *Appl. Phys.* **2**, 45–46 (1973)
71. A.K. Jain, V.N. Kulkarni, D.K. Sood, J.S. Uppal, Periodic surface ripples in laser-treated aluminum and their use to determine absorbed power. *J. Appl. Phys.* **52**, 4882–4884 (1981)
72. F. Keilmann, Y.H. Bai, Periodic surface structures frozen into CO₂ laser-melted quartz. *Appl. Phys. A* **29**, 9–18 (1982)
73. Z. Guosheng, P.M. Fauchet, A.E. Siegman, Growth of spontaneous periodic surface structures on solids during laser illumination. *Phys. Rev. B* **26**, 5366–5381 (1982)
74. J.E. Sipe, J.F. Young, J.S. Preston, H.M. van Driel, Laser-induced periodic surface structure. I. Theory. *Phys. Rev. B* **27**, 1141–1154 (1983)
75. J.F. Young, J.S. Preston, H.M. van Driel, J.E. Sipe, Laser-induced periodic surface structure. II. Experiments on Ge, Si, Al, and brass. *Phys. Rev. B* **27**, 1155–1172 (1983)
76. J.F. Young, J.E. Sipe, H.M. van Driel, Laser-induced periodic surface structure. III. Fluence regimes, the role of feedback, and details of the induced topography in germanium. *Phys. Rev. B* **30**, 2001–2015 (1984)

77. M. Bolle, S. Lazare, M. Le Blanc, A. Wilmes, Submicron periodic structures produced on polymer surfaces with polarized excimer laser ultraviolet radiation. *Appl. Phys. Lett.* **60**(1992), 674–676 (1992)
78. A.M. Ozkan, A.P. Malshe, T.A. Railkar, W.D. Brown, M.D. Shirk, P.A. Molian, Femtosecond laser-induced periodic structure writing on diamond crystals and microclusters. *Appl. Phys. Lett.* **75**, 3716–3718 (1999)
79. A. Borowiec, H.K. Haugen, Subwavelength ripple formation on the surfaces of compound semiconductors irradiated with femtosecond laser pulses. *Appl. Phys. Lett.* **82**, 4462–4464 (2003)
80. J. Wang, C. Guo, Ultrafast dynamics of femtosecond laser-induced periodic surface pattern formation on metals. *Appl. Phys. Lett.* **87**, 251914 (2005)
81. E. Rebollar, J.R. Vazquez de Aldana, J.A. Perez-Hernandez, T.A. Ezquerro, P. Moreno, M. Castillejo, Ultraviolet and infrared femtosecond laser induced periodic surface structures on thin polymer films. *Appl. Phys. Lett.* **100**, 041106 (2012)
82. A.Y. Vorobyev, Chunlei Guo, Femtosecond laser structuring of titanium implants. *Appl. Surf. Sci.* **253**, 7272–7280 (2007)
83. P. Gregorčič, M. Sedlaček, B. Podgornik, J. Reif, Formation of laser-induced periodic surface structures (LIPSS) on toolsteel by multiple picosecond laser pulses of different polarizations. *Appl. Surf. Sci.* **387**, 698–706 (2016)
84. K.R.P. Kafka, D.R. Austin, H. Li, A.Y. Yi, J. Cheng, E.A. Chowdhury, Time-resolved measurement of single pulse femtosecond laser-induced periodic surface structure formation induced by a pre-fabricated surface groove. *Opt. Express* **23**, 19432–19441 (2015)
85. J. Reif, O. Varlamova, S. Uhlig, S. Varlamov, M. Bestehorn, On the physics of self-organized nanostructure formation upon femtosecond laser ablation. *Appl. Phys. A* **117**, 179–184 (2014)
86. E.L. Gurevich, Mechanisms of femtosecond LIPSS formation induced by periodic surface temperature modulation. *Appl. Surf. Sci.* **374**, 56–60 (2016)
87. O. Varlamova, F. Costache, M. Ratzke, J. Reif, Control parameters in pattern formation upon femtosecond laser ablation. *Appl. Surf. Sci.* **253**, 7932–7936 (2007)
88. J. Reif, *Basic Physics of Femtosecond Laser Ablation*, Ch. 2, eds. by A. Miotello, P. Ossi. *Laser-Surface Interactions for New Materials Production*; Springer Ser. Mater. Sci. **130** (Springer, Berlin Heidelberg, 2010)
89. J. Reif, O. Varlamova, F. Costache, Femtosecond laser induced nanostructure formation: self-organization control parameters. *Appl. Phys. A* **92**, 1019–1024 (2008)
90. J. Reif, *Processing with Ultrashort Laser Pulses*, ch. 6, ed. by P. Schaaf. *Laser Processing of Materials*, Springer Ser. Mater. Sci. vol 139 (Springer, Berlin, Heidelberg, 2010), pp. 113–129
91. O. Varlamova, C. Martens, M. Ratzke, J. Reif, Genesis of femtosecond-induced nanostructures on solid surfaces. *Appl. Opt.* **53**, I 10-I 15 (2014)
92. O. Varlamova, M. Bounhalli, J. Reif, Influence of irradiation dose on laser-induced surface nanostructures on silicon. *Appl. Surf. Sci.* **278**, 62–66 (2002)
93. A.-M. Kietzig, M.N. Mirvakili, S. Kamal, P. Englezos, S.G. Hatzikiriakos, Laser-patterned super-hydrophobic pure metallic substrates: Cassie to Wenzel Wetting Transitions. *J. Adhes. Sci. Technol.* **25**, 2789–2809 (2011)
94. J. Gottmann, R. Wagner, Sub-wavelength ripple formation on dielectric and metallic materials induced by tightly focused femto-second laser radiation. *Proc. SPIE* **6106**, 61061R (2006)
95. M. Gedvilas, G. Račiukaitis, K. Regelskis, P. Gečys, Formation of gratings by self-organization of the chromium thin film on the glass substrate under irradiation with laser pulses. *JLMN* **3**, 58–62 (2008)
96. M. Hörstmann-Jungemann, J. Gottmann, D. Wortmann, Nano- and microstructuring of SiO₂ and sapphire with Fs-laser induced selective etching. *JLMN* **4**, 135–140 (2009)
97. M. Zamfirescu, M. Ulmeanu, F. Jipa, O. Cretu, A. Moldovan, G. Epurescu, M. Dinescu, R. Dabu, Femtosecond laser induced periodic surface structures on ZnO thin films. *JLMN* **4**, 7–10 (2009)
98. J. Reif, *Material Response to Laser Energy Deposition (Thermal and Hyperthermal Processes)*, ch. 2 eds. by M. Castillejo, P. Ossi, L. Zhigilei. *Lasers in Materials Science*; Springer Ser. Mater. Sci. vol 191 (Springer, Berlin, Heidelberg, 2014)

99. V. Zorba, L. Persano, D. Pisignano, A. Athanassiou, E. Stratakis, R. Cingolani, P. Tzanetakis, C. Fotakis, Making silicon hydrophobic: wettability control by two-lengthscale simultaneous patterning with femtosecond laser irradiation. *Nanotechnology* **17**, 3234 (2006)
100. M. Groenendijk, J. Meijer, Microstructuring using femtosecond pulsed laser ablation. *J. Laser Appl.* **18**, 227–235 (2006)
101. M. Groenendijk, Fabrication of super hydrophobic surfaces by fs laser pulses. *Laser Technol. J.* **5**, 44–47 (2008)
102. M. Barberoglou, V. Zorba, E. Stratakis, E. Spanakis, P. Tzanetakis, S.H. Anastasiadis, C. Fotakis, Bio-inspired water repellent surfaces produced by ultrafast laser structuring of silicon. *Appl. Surf. Sci.* **255**, 5425–5429 (2009)
103. P. Bizi-Bandoki, S. Benayoun, S. Valette, B. Beaugiraud, E. Audouard, Modifications of roughness and wettability properties of metals induced by femtosecond laser treatment. *Appl. Surf. Sci.* **257**, 5213–5218 (2011)
104. A.Y. Vorobyev, C. Guo, Metal pumps liquid uphill. *Appl. Phys. Lett.* **94**, 224102 (2009)
105. A.Y. Vorobyev, C. Guo, Laser turns silicon superwicking. *Opt. Express* **18**, 6455–6460 (2010)
106. J.J. Yu, Y.F. Lu, Laser-induced ripple structures on Ni-P substrates. *Appl. Surf. Sci.* **148**, 248–252 (1999)
107. A. Mizuno, T. Honda, J. Kikuchi, Y. Iwai, N. Yasumaru, K. Miyazaki, Friction properties of the DLC film with periodic structures in nano-scale. *Tribol. Online* **1**, 44–48 (2006)
108. N. Yasumaru, K. Miyazaki, J. Kiuchi, Control of tribological properties of diamond-like carbon films with femtosecond-laser-induced nanostructuring. *Appl. Surf. Sci.* **254**, 2364–2368 (2008)
109. C.Y. Chen, C.J. Chung, B.H. Wu, W.L. Li, C.W. Chien, P.H. Wu, C.W. Cheng, Microstructure and lubricating property of ultra-fast laser pulse textured silicon carbide seals. *Appl. Phys. A* **107**, 345–350 (2012)
110. J. Eichstadt, G.R.B.E. Romer, A.J. Huis in't Veld, Towards friction control using laser-induced periodic surface structures. *Phys. Procedia* **12**, 7–15 (2011)
111. S. Hammouti, A. Pascale-Hamri, N. Faure, B. Beaugiraud, M. Guibert, C. Mauclair, S. Benayoun, S. Valette, Wear rate control of peek surfaces modified by femtosecond laser. *Appl. Surf. Sci.* **357**, 1541–1551 (2015)
112. J. Dufils, F. Faverjon, C. Héau, C. Donnet, S. Benayoun, S. Valette, Combination of laser surface texturing and DLC coating on PEEK for enhanced tribological properties. *Surf. Coat. Technol.* **329**, 29–41 (2017)
113. J. Bonse, R. Koter, M. Hartelt, D. Spaltmann, S. Pentzien, S. Höhm, A. Rosenfeld, J. Krüger, Tribological performance of femtosecond laser-induced periodic surface structures on titanium and a high toughness bearing steel. *Appl. Surf. Sci.* **336**, 21–27 (2015)
114. J. Bonse, S. Höhm, R. Koter, M. Hartelt, D. Spaltmann, S. Pentzien, A. Rosenfeld, J. Krüger, Tribological performance of sub-100-nm femtosecond laser-induced periodic surface structures on titanium. *Appl. Surf. Sci.* **374**, 190–196 (2016)
115. J. Reif, O. Varlamova, M. Ratzke, M. Schade, H.S. Leipner, Tz Arguirov, Multipulse feedback in self-organized ripples formation upon femtosecond laser ablation from silicon. *Appl. Phys. A* **101**, 361–365 (2010)
116. E. Rebolgar, M. Sanz, S. Pérez, M. Hernández, I. Martín-Fabiani, D.R. Rueda, T.A. Ezquerria, C. Domingo, M. Castillejo, Gold coatings on polymer laser induced periodic surface structures: assessment as substrates for surface-enhanced Raman scattering. *Phys. Chem. Chem. Phys.* **14**, 15699–15705 (2012)
117. H. Messaoudi, S. Kumar Das, J. Lange, F. Heinrich, S. Schrader, M. Frohme, R. Grunwald, *Femtosecond-Laser Induced Periodic Surface Structures for Surface Enhanced Raman Spectroscopy of Biomolecules*, eds. by S. Sakabe, C. Lienau, R. Grunwald. *Progress in Nonlinear Nano-Optics* (Springer, Cham, 2015), pp. 207–2019
118. R. Buividas, P. Stoddart, S. Juodkakis, Laser fabricated ripple substrates for surface-enhanced Raman scattering. *Ann. Phys.* **524**, L5–L10 (2012)
119. R. Vilar (ed.), *Laser Surface Modification of Biomaterials—Techniques and Applications*; Woodhead Publ. Ser. Biomat. **111** (Elsevier, Duxford, 2016)

120. Y.F. Guan, A.V. Melechko, A.J. Pedraza, L.R. Baylor, P.D. Rack, Maskless synthesis of Vertically Aligned Carbon Nanofibers (VACNF) field emission arrays on a Laser-Induced Periodic Surface Structures (LIPSS) template, in *Proceeding of 20th International Vacuum Nanoelectronics Conference*, pp. 143–144, 2007
121. A. Ranella, M. Barberoglou, S. Bakogianni, C. Fotakis, E. Stratakis, Tuning cell adhesion by controlling the roughness and wettability of 3D micro/nano silicon structures. *Acta Biomater.* **6**, 2711–2720 (2010)
122. E.L. Papadopoulou, A. Samara, M. Barberoglou, A. Manousaki, S.N. Pagakis, E. Anastasiadou, C. Fotakis, E. Stratakis, Silicon scaffolds promoting three-dimensional neuronal web of cytoplasmic processes. *Tissue Eng.* **16**, 497–502 (2010)
123. T. Shinonaga, M. Tsukamoto, T. Kawa, P. Chen, A. Nagai, T. Hanawa, Formation of periodic nanostructures using a femtosecond laser to control cell spreading on titanium. *Appl. Phys. B* **119**, 493–496 (2015)
124. J. Bonse, A. Rosenfeld, J. Krüger, On the role of surface plasmon polaritons in the formation of laser-induced periodic surface structures upon irradiation of silicon by femtosecond-laser pulses. *J. Appl. Phys.* **106**, 104910 (2009)
125. O. Varlamova, J. Reif, S. Varlamov, M. Bestehorn, *Self-organized Surface Patterns Originating from Laser-Induced Instability*; ch. 1 eds. by S. Sakabe, C. Lienau, R. Grunwald. *Progress in Nonlinear Nano-Optics*; Springer Ser. Nano-Opt. Nanophot, vol 2 (2015)
126. J. Reif, O. Varlamova, S. Varlamov, M. Bestehorn, 2012, The role of asymmetric excitation in self-organized nanostructure formation upon femtosecond laser ablation. *AIP Conf. Proc.* **1464**, 428–441 (2012)